SFB 823

Bayesian prediction for a jump diffusion process

with application to crack growth in fatigue experiments

Simone Hermann, Katja Ickstadt, Christine H. Müller

Nr. 30/2015

Discussion Paper

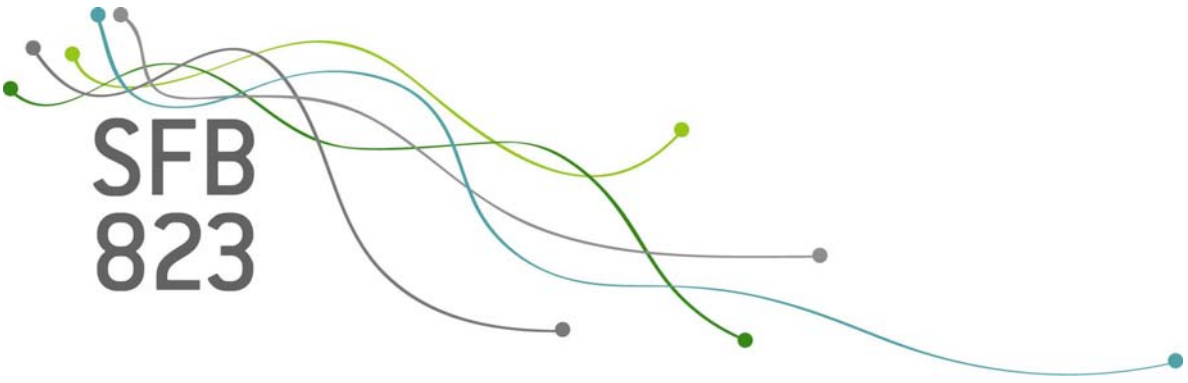

Bayesian prediction for a jump diffusion process

with application to crack growth in fatigue experiments

Simone Hermann*, Katja Ickstadt*, Christine H. Müller*

August 18, 2015

In many fields of technological developments, understanding and controlling material fatigue is an important point of interest. This article is concerned with statistical modeling of the damage process of prestressed concrete under low cyclic load. A crack width process is observed which exhibits jumps with increasing frequency. Firstly, these jumps are modeled using a Poisson process where two intensity functions are presented and compared. Secondly, based on the modeled jump process, a stochastic process for the crack width is considered through a stochastic differential equation (SDE). It turns out that this SDE has an explicit solution. For both modeling steps, a Bayesian estimation and prediction procedure is presented.

Keywords: Nonhomogeneous Poisson process (NHPP), crack growth, Bayesian estimation, predictive distribution.

1. Introduction

In constructional engineering, material fatigue is a relevant topic of research because it is important to predict the lifetime of, for example, bridges. Experiments in this field, especially under low loadings, are very rare because they are very expensive and take very long, at times over several months. Maurer and Heeke (2010) carried out five experiments where prestressed concrete beams with initial cracks have been put under cyclic load. Recently, two new experiments were conducted, see Heeke et al. (2015). All seven data series are considered here. Each prestressed concrete beam contains 35 tension wires which usually break at different time points. Therefore, the resulting crack widths which can be seen in Figure 1 for two of the experiments, exhibit jumps with increasing frequency that influence the crack growth process substantially. Structure-borne noise measurements during the experiments provide information concerning the break times of the tension wires which match the observed jumps in the crack width data. This finding has important implications for the estimation procedure.

*TU Dortmund University, Faculty of Statistics, Vogelpothsweg 87, D-44221 Dortmund, Germany, hermann@statistik.tu-dortmund.de

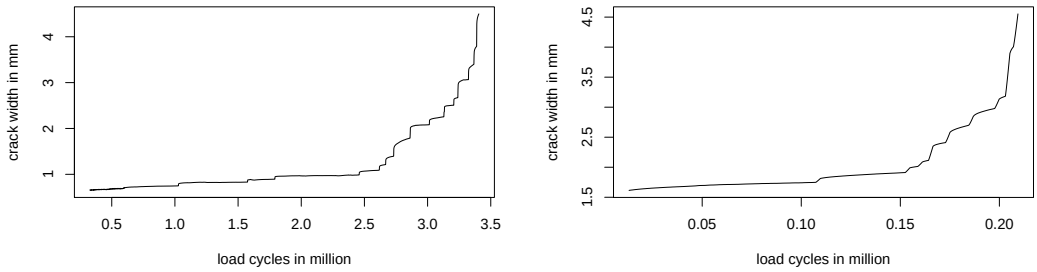

Figure 1: Crack width data resulting from the first two experiments of Maurer and Heeke (2010)

A model often used for crack growth in the engineering literature is the deterministic process defined by the Paris-Erdogan equation

$$\frac{da}{dN} = C(\Delta K)^m \tag{1}$$

where a denotes the crack length, N the number of cycles corresponding to the crack length a, while C and m are material constants. ΔK denotes the stress intensity factor range that depends on the square root of a. That leads to an autoregressive process whose differences increase with the growth of the process itself. For further information see, for example, Sobczyk and Spencer (1992). Because any process resulting from this equation will be deterministic and, therefore, will not describe the uncertainties of the growth process, this approach will be extended in the remainder.

A diffusion model would be one extension of the ordinary differential equation in (1). A Bayesian approach for growth diffusions is investigated in Hermann et al. (2015) within a hierarchical model and applied to a data set of experiments in aluminum alloy which is a homogeneous material in contrast to concrete. Therefore, we need some additional approach for modeling the irregular jumps in the concrete data. In Heeke et al. (2015), the underlying jump process is modeled by a nonhomogeneous Poisson process (NHPP), which is embedded in a nonlinear regression model. Of course, other jump processes are possible, but the NHPP is a good starting point because we observe very few jumps and cannot, therefore, estimate many parameters. Since we observe an increasing frequency of the jumps, a homogeneous process would not be able to predict reliably. Therefore, a NHPP is reasonable. A two-parameter approach for the intensity was used in Heeke et al. (2015) and provided good results. Instead of the nonlinear regression model for the concrete crack width, in the following we introduce a more intuitive process model; it is defined by a stochastic differential equation (SDE) that extends the Paris-Erdogan equation (1) and includes the NHPP which fits the jumps in the data. In the Bayesian estimation scheme, the fact of known event times of the jump process will be important. Otherwise the approach would yield a hidden Markov model and a challenge would be to estimate, i.e. filter, the jump process. Based on samples from the posterior distribution, a predictive distribution for the NHPP as well as for the jump diffusion process will be presented. This distribution provides point prediction as well as prediction intervals.

NHPPes are well-known in the literature. A good overview of the Bayesian analysis can be found in Ríos Insua et al. (2012). Meeker and Escobar (1998), for example, present maximum likelihood estimators for several intensity functions and give a historical overview of the literature employing NHPPes in reliabilty theory, see pp. 413–420. Sobczyk and Spencer (1992) introduce cumulative jump models based on homogeneous and nonhomogeneous Poisson processes to describe crack growth as a discontinuous random process. A Bayesian approach for NHPPes can be found in Kuo and Yang (1996) with application in software reliability, in Yuan et al. (2009) for modeling pitting corrosion in steam generator tubes and in Pievatolo and Ruggeri (2004) for reliability of complex repairable systems.

One possibility to include the counting process into a whole framework for the crack width is to use the ideas of Chiquet et al. (2009) where a piecewise deterministic Markov process is investigated. Since they use a stationary Markov process with finite state space, their approach is not directly applicable to our case. The approach presented in the following is based on the ideas by Bodo et al. (1987) and Shimizu and Yoshida (2006), respectively, who both take the SDE of a diffusion process and add a term for the jumps which yields a jump diffusion model. Both assume a homogeneous Poisson process and Shimizu and Yoshida (2006) assume an ergodic process which is not suitable for our data, but the idea of the process will be borrowed. Rifo and Torres (2009) present a Bayesian significance test for jump detection in a diffusion process. However, in our data set, the jumps are observed because of sound measurements determining the tension wires' breaking. An overview of so-called jump diffusion processes is given in Øksendal and Sulem (2005). All in all, the employed jump diffusion process fits in the framework of Lévy jump processes but with nonstationary increments because of the increasing frequency of the Poisson process.

In this paper, a novel two-stage modeling procedure is presented. Firstly, the posterior distribution of the NHPP's intensity rate parameters is approximated with a MCMC sampler and integrated in the predictive distribution of the NHPP, which itself is approximated by drawing from a sampling procedure. Secondly, the posterior distribution of the parameters in the jump diffusion process, modeling the crack width, is approximated by samples drawn by a Gibbs sampler. These parameter samples and the counting process samples, drawn from the predictive distribution obtained in the first modeling step, are employed to approximate the predictive distribution for the jump diffusion process, i.e. the crack width curve.

The remainder of this work is structured as follows: In the next section, the two-stage model is presented and the Bayesian estimation and prediction procedure is employed, in Subsection 2.1 for the NHPP and in Subsection 2.2 for the model describing the crack width. Section 3 displays the results for the crack width data. Afterwards, Section 4 sums up and gives a short outlook.

2. Modeling, estimation and prediction

2.1. Poisson process

The first important modeling step is to describe the wire failure process, which by construction is a counting process. When resorting to the most widely used counting process, i.e. the Poisson process, it is clear that a nonhomogeneous specification has to be employed: When a tension wire fails, the load distributes on fewer wires and, therefore, the probability of another wire failure grows. Denoting the number of broken wires at time t with N_t we assume the process to start at 0, i.e. $N_0 = 0$ almost surely. The differences are independent, i.e. for

arbitrary $0 \leq t_1 < ... < t_n$ the increments $N_{t_2} - N_{t_1}, ..., N_{t_n} - N_{t_{n-1}}$ are independent, and Poisson distributed, i.e. for all $0 \leq s < t$: $N_t - N_s$ is Poisson distributed with parameter $\int_s^t \lambda_\xi(u)\, du$. This leads to a NHPP $\{N_t,\ t \in [0, \infty)\}$ with intensity rate $\lambda_\xi(t)$. We will compare two different types of $\mathbb{E}[N_t] = \int_0^t \lambda_\xi(u)\, du =: \Lambda_\xi(t)$, one for polynomial and one for exponential growth:

$$\Lambda_\xi(t) = \left(\frac{t}{\beta}\right)^\alpha, \qquad \xi = (\alpha, \beta) \in [1, \infty) \times (0, \infty) \tag{2}$$

$$\Lambda_\xi(t) = \exp(at + c) - \exp(c), \qquad \xi = (a, c) \in (0, \infty) \times \mathbb{R}, \tag{3}$$

where function (2) has the nice property that the derivative of $\Lambda_\xi(t)$ is the hazard rate of the Weibull distribution and the homogeneous case of the process is nested by setting $\alpha = 1$. This specification is also known as power law in the literature, see for example Yu et al. (2007). The second function (3) represents an exponential intensity rate that takes up the idea of the Paris-Erdogan equation (1) with the special case of $m = 2$. This equation would lead to a function $f(t) = b \exp(at)$ which is just another parameterization for the derivative of the function in (3). Of course, one could try an approach based on the general Paris-Erdogan equation with a third parameter m. However, some experiments we use for prediction consist of four or five observed event times which makes it difficult to estimate more than two parameters.

Based on the event times $0 < T_1 < ... < T_m < T$ with $T_i = \min\{s :\ N_s = i\}$ and T the last observation time point, the likelihood is given by

$$p(T_1, ..., T_m |\ \xi) = \exp(-\Lambda_\xi(T)) \prod_{i=1}^{m} \lambda_\xi(T_i),$$

see, e.g., Ríos Insua et al. (2012) p. 119. There is no obvious conjugate prior distribution for ξ so we will use the Metropolis-Hastings (MH) algorithm, see Robert and Casella (2004) p. 270. The employed proposal density is described in the Appendix, Section B.1. In our application, we use a noninformative approach without any prior information.

Based on the MH-resulting samples $\xi_1^*, ..., \xi_K^* \sim p(\xi |\ T_1, ..., T_m)$, the following predictive distribution for the next event time can be approximated by

$$\begin{aligned} p(T_{m+1}^* |\ T_1, ..., T_m) &= \int p(T_{m+1}^* |\ T_m, \xi) \cdot p(\xi |\ T_1, ..., T_m)\, d\xi \\ &= \int \lambda_\xi(T_{m+1}^*) \exp\left(-\{\Lambda_\xi(T_{m+1}^*) - \Lambda_\xi(T_m)\}\right) \cdot p(\xi |\ T_1, ..., T_m)\, d\xi \\ &\approx \frac{1}{K} \sum_{k=1}^{K} \lambda_{\xi_k^*}(T_{m+1}^*) \exp\left(-\{\Lambda_{\xi_k^*}(T_{m+1}^*) - \Lambda_{\xi_k^*}(T_m)\}\right). \end{aligned}$$

For predicting a trajectory, we need more than one next event time. Therefore, we approxi-

mate the predictive distribution for $i \geq 2$

$$\begin{aligned} p(T^*_{m+i}|T^*_{m+i-1}, T_1, ..., T_m) &= \int p(T^*_{m+i}|T^*_{m+i-1}, \xi) p(\xi|T^*_{m+i-1}, T_1, ..., T_m)\, d\xi \\ &\approx \int p(T^*_{m+i}|T^*_{m+i-1}, \xi) p(\xi|T_1, ..., T_m)\, d\xi \\ &\approx \frac{1}{K} \sum_{k=1}^{K} p(T^*_{m+i}|T^*_{m+i-1}, \xi^*_k) \\ &= \frac{1}{K} \sum_{k=1}^{K} \lambda_{\xi^*_k}(T^*_{m+i}) \exp\left(-\{\Lambda_{\xi^*_k}(T^*_{m+i}) - \Lambda_{\xi^*_k}(T^*_{m+i-1})\}\right), \end{aligned} \tag{4}$$

which leads to trajectory samples $T_m < T^{*(l)}_{m+1} < T^{*(l)}_{m+2} < ...$ until $T^{*(l)}_{m+i}$ arrives some fixed t^*, $l = 1, ..., L$. The number of event times differs for each trajectory, because the number of jumps N_{t^*} is random and varies for each path. The practical implementation of this sampling procedure is explained in the appendix, Section B.2.

The trajectory samples of the Poisson process can be calculated as follows

$$N^{*(l)}_t = \{j : T^{*(l)}_j \leq t < T^{*(l)}_{j+1}\},\ l = 1, ..., L. \tag{5}$$

In the following, point predictions will be given by the pointwise median of these sampled processes and interval predictions by the pointwise $\frac{\alpha}{2}$– and $(1 - \frac{\alpha}{2})$– quantiles.

2.2. Jump diffusion process

Inference for the wire failure process is a key input for the next step, where we intend to investigate the crack width process. This process is modeled by a SDE of the form

$$dX_t = \phi X_t\, dt + \gamma X_t\, dW_t + \theta X_t\, dN_t, \tag{6}$$

with some constant initial value x_0 and $\{W_t,\ t \in [0, \infty)\}$ denoting a Wiener process which has to be independent of the NHPP $\{N_t,\ t \in [0, \infty)\}$. Assuming $\phi, \gamma, \theta > 0$ and a positive starting value leads to a growth process almost surely. This is a stochastic extension of the simplified version of the Paris-Erdogan equation $dX_t = \phi X_t\, dt$ as mentioned above in (1). The SDE in (6) has a unique strong solution given by

$$X_t = x_0 \cdot \exp\left(\phi t - \frac{\gamma^2}{2} t + \gamma W_t + \log(1 + \theta) N_t\right). \tag{7}$$

This can be seen by direct calculation using Itô's formula for noncontinuous semimartingales, see Protter (2005) p. 79, and is, for example, employed in Øksendal and Sulem (2005), p. 7 in example 1.15.

We get the Bayesian model

$$\begin{aligned} \log(X_{t_i})|N_{t_i}, \phi, \gamma^2, \theta &\sim \mathcal{N}(\log(x_0) + (\phi - \frac{\gamma^2}{2})t_i + \log(1 + \theta) N_{t_i}, \gamma^2 t_i) \\ N_{t_i} &\sim \text{Pois}(\Lambda_\xi(t_i)),\ i = 1, ..., n \\ \phi &\sim \mathcal{N}(m^{\text{prior}}_\phi, v^{\text{prior}}_\phi) \\ \gamma^2 &\sim IG(a^{\text{prior}}, b^{\text{prior}}) \\ \widetilde{\theta} := \log(1 + \theta) &\sim \mathcal{N}(m^{\text{prior}}_\theta, v^{\text{prior}}_\theta). \end{aligned} \tag{8}$$

For the whole data vector $\eta = (\phi, \widetilde{\theta}, \gamma^2)$, this leads to a multivariate normal likelihood for the logarithms

$$(\log(X_{t_1}), ..., \log(X_{t_n}))|\ \eta, N_{t_1}, ..., N_{t_n} \sim \mathcal{N}(\mu_n(\eta),\ \gamma^2 T_n),$$

where $\mu_n(\eta) = \log(x_0) \cdot 1_n + (\phi - \frac{\gamma^2}{2}) \cdot (t_1, ..., t_n) + \widetilde{\theta} \cdot (N_{t_1}, ..., N_{t_n})$, $T_n = (\min(t_i, t_j))_{i,j=1,...,n}$ and $1_n = (1, ..., 1) \in \mathbb{R}^n$. In the following, denote with $t_{(n)}$ the vector $(t_1, ..., t_n)$, with $\log(X)_{(n)}$ the vector $(\log(X_{t_1}), ..., \log(X_{t_n}))$, and with $N_{(n)}$ the vector $(N_{t_1}, ..., N_{t_n})$.

Estimation of ϕ and $\widetilde{\theta}$ is simplified by the fact that the normal prior is conjugate to the multivariate normal likelihood. The full conditional posterior for ϕ is given by

$$\begin{aligned}
&\phi|\ \log(X)_{(n)}, N_{(n)}, \widetilde{\theta}, \gamma^2 \sim \mathcal{N}(m_\phi^{\text{post}}, v_\phi^{\text{post}}) \\
&v_\phi^{\text{post}} = \left(\frac{1}{\gamma^2} t_{(n)} T_n^{-1} t_{(n)}^T + \frac{1}{v_\phi^{\text{prior}}} \right)^{-1} \\
&m_\phi^{\text{post}} = v_\phi^{\text{post}} \left\{ \frac{m_\phi^{\text{prior}}}{v_\phi^{\text{prior}}} + \frac{1}{\gamma^2} t_{(n)} T_n^{-1} \left(\log(X)_{(n)} - \log(x_0) 1_n + \frac{\gamma^2}{2} t_{(n)} - \widetilde{\theta} N_{(n)} \right)^T \right\}
\end{aligned}$$

and for $\widetilde{\theta}$ by

$$\begin{aligned}
&\widetilde{\theta}|\ \log(X)_{(n)}, N_{(n)}, \phi, \gamma^2 \sim \mathcal{N}(m_\theta^{\text{post}}, v_\theta^{\text{post}}) \\
&v_\theta^{\text{post}} = \left(\frac{1}{\gamma^2} N_{(n)} T_n^{-1} N_{(n)}^T + \frac{1}{v_\theta^{\text{prior}}} \right)^{-1} \\
&m_\theta^{\text{post}} = v_\theta^{\text{post}} \cdot \left\{ \frac{m_\theta^{\text{prior}}}{v_\theta^{\text{prior}}} + \frac{1}{\gamma^2} N_{(n)} T_n^{-1} \left(\log(X)_{(n)} - \log(x_0) 1_n - (\phi - \frac{\gamma^2}{2}) t_{(n)} \right)^T \right\}.
\end{aligned}$$

For the estimation of γ^2 with the prior density $p(\gamma^2) = \frac{b^{\text{prior}}}{\Gamma(a^{\text{prior}})} (\gamma^2)^{-a^{\text{prior}}-1} \exp\left(-\frac{b^{\text{prior}}}{\gamma^2}\right)$ we calculate the conditional posterior density

$$\begin{aligned}
&p(\gamma^2|\ \log(X)_{(n)}, N_{(n)}, \phi, \widetilde{\theta}) \\
\propto &(\gamma^2)^{-(\frac{n}{2} + a^{\text{prior}}) - 1} \cdot \\
&\exp\left(-\frac{1}{\gamma^2} \left\{ \frac{1}{2} (\log(X)_{(n)} - \mu_n(\eta)) T_n^{-1} (\log(X)_{(n)} - \mu_n(\eta))^T + b^{\text{prior}} \right\} \right).
\end{aligned}$$

Since $\mu_n(\eta)$ also depends on γ^2, its posterior is not an inverse Gamma distribution. But we can conduct a Metropolis Hastings step within the Gibbs sampler and use the inverse Gamma as proposal density. With $\mu_{n,\phi,\widetilde{\theta}}(\gamma^2) := \mu_n(\eta)$, define

$$\begin{aligned}
q(\gamma^2|\widetilde{\gamma}^2, \phi, \widetilde{\theta}) = &(\gamma^2)^{-(\frac{n}{2} + a^{\text{prior}}) - 1} \\
&\cdot \exp\left(-\frac{1}{\gamma^2} \left\{ \frac{1}{2} (\log(X)_{(n)} - \mu_{n,\phi,\widetilde{\theta}}(\widetilde{\gamma}^2)) T_n^{-1} (\log(X)_{(n)} - \mu_{n,\phi,\widetilde{\theta}}(\widetilde{\gamma}^2))^T + b^{\text{prior}} \right\} \right),
\end{aligned}$$

which is proportional to an inverse Gamma density of γ^2 dependent on $\widetilde{\gamma}^2$. The Metropolis Hastings step in the kth iteration begins with drawing from the proposal

$$\gamma^2_{\text{cand}} \sim q(\gamma^2|\gamma^{2*}_{k-1}, \phi^*_{k-1}, \widetilde{\theta}^*_{k-1}),$$

which is accepted with probability

$$\min\left\{1,\ \frac{p(\gamma^2_{\text{cand}}|\ \log(X)_{(n)}, N_{(n)}, \phi^*_{k-1}, \widetilde{\theta}^*_{k-1}) q(\gamma^{2*}_{k-1}|\gamma^2_{\text{cand}}, \phi^*_{k-1}, \widetilde{\theta}^*_{k-1})}{p(\gamma^{2*}_{k-1}|\ \log(X)_{(n)}, N_{(n)}, \phi^*_{k-1}, \widetilde{\theta}^*_{k-1}) q(\gamma^2_{\text{cand}}|\gamma^{2*}_{k-1}, \phi^*_{k-1}, \widetilde{\theta}^*_{k-1})}\right\}$$
$$= \min\left\{1,\ \exp\left(\frac{1}{2}\left(\frac{1}{\gamma^{2*}_{k-1}} + \frac{1}{\gamma^2_{\text{cand}}}\right)\right.\right.$$
$$\left.\left.\cdot\left((\gamma^{2*}_{k-1} - \gamma^2_{\text{cand}}) t_{(n)} T_n^{-1} C_n^T + \frac{1}{4}((\gamma^{2*}_{k-1})^2 - (\gamma^2_{\text{cand}})^2) t_{(n)} T_n^{-1} t_{(n)}^T\right)\right)\right\}.$$

The full calculation can be seen in Appendix A. The Gibbs sampler unites the three estimation steps as follows

$$\begin{aligned}
\phi^*_k &\sim p(\phi|\ \log(X)_{(n)}, N_{(n)}, \widetilde{\theta}^*_{k-1}, \gamma^{2*}_{k-1}) \\
\widetilde{\theta}^*_k &\sim p(\widetilde{\theta}|\ \log(X)_{(n)}, N_{(n)}, \phi^*_k, \gamma^{2*}_{k-1}) \\
\gamma^{2*}_k &\sim p(\gamma^2|\ \log(X)_{(n)}, N_{(n)}, \phi^*_k, \widetilde{\theta}^*_k),\ k = 1, ..., K.
\end{aligned}$$

In a last step, we calculate the predictive density $p(X_{t^*}|\ X_{(n)}, N_{(n)})$ for $t^* > t_n$. From the solution (7) it becomes clear that the logarithm of X_{t^*} conditional upon N_{t^*} is normally distributed with mean $\log(x_0) + (\phi - \frac{\gamma^2}{2})t^* + \widetilde{\theta} N_{t^*}$ and variance $\gamma^2 t^*$. The solution (7) is a first order Markov process, which implies that

$$\log(X_{t^*})|\ \log(X_{t_n}), N_{t_n}, N_{t^*}, \eta$$
$$\sim \mathcal{N}\left((\log(X_{t_n}) + (\phi - \frac{\gamma^2}{2})(t^* - t_n) + \widetilde{\theta}(N_{t^*} - N_{t_n}),\ \gamma^2(t^* - t_n)\right).$$

This leads to the predictive distribution

$$\begin{aligned}
&p(\log(X_{t^*})|\ X_{(n)}, N_{(n)}) \qquad (9)\\
&= \int p(\log(X_{t^*})|\ \log(X_{t_n}), N_{t_n}, N_{t^*}, \eta) \cdot p(\eta|\ X_{(n)}, N_{(n)}) \cdot p(N_{t^*}|\ N_{(n)})\, d(\eta, N_{t^*}) \\
&\approx \frac{1}{K}\sum_{k=1}^{K} p(\log(X_{t^*})|\ \log(X_{t_n}), N_{t_n}, N^{(k)}_{t^*}, \eta^*_k),
\end{aligned}$$

where $\eta^*_k = (\phi^*_k, \widetilde{\theta}^*_k, \gamma^{2*}_k),\ k = 1, ..., K$, are the posterior samples from the Gibbs sampler and $N^{(k)}_{t^*}$ the samples from the predictive distribution of the counting process as seen in (5) with $L = K$. Sampling from (9) can be realised by a rejection sampling method, see, for example, Robert and Casella (2004), p. 47. Here, we only sample pointwise from a univariate distribution. An alternative would be sampling trajectories of the process. Non-Bayesian trajectory simulation methods for jump diffusion processes can be found in Casella and Roberts (2011) or Giesecke and Smelov (2013). The corresponding Bayesian formulation for trajectory prediction will be future work.

3. Application to crack growth in prestressed concrete

In the following we will apply the proposed method to the data set mentioned in the introduction. Two experiments can be seen in Figure 1 whereas a detailed explanation of the whole

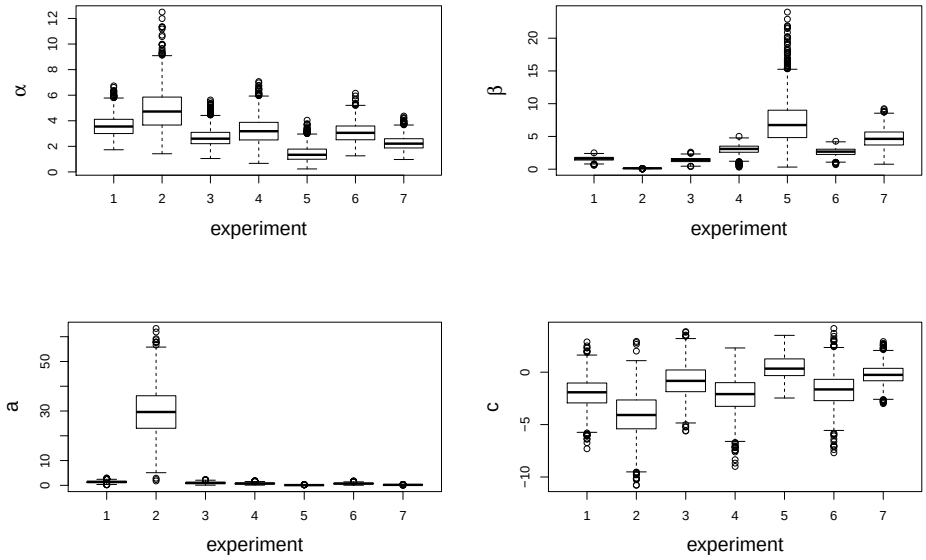

Figure 2: Boxplots of the posterior distributions for α and β in the case of $\Lambda_\xi(t) = \left(\frac{t}{\beta}\right)^\alpha$ (top) and for a and c in the case of $\Lambda_\xi(t) = \exp(at + c) - \exp(c)$ (bottom) of the NHPP

data set can be found in Heeke et al. (2015). For all estimations, we divide the number of load cycles by one million to avoid numerical problems. Since we assume a time-continuous process, we could also take the observed time in seconds, but in the engineering literature the number of load cycles is usually chosen as the independent variable. For the estimation of the intensity rate parameter ξ, we take the number of load cycles in million up to the wire failures as event times which are observed in the seven experiments. To get good starting values for the MH algorithm, we take a grid ($\alpha \in [1, 5],\ \beta \in [0.1, 8]$ and $a \in [0, 3],\ c \in [-5, 1]$, each with distance of 0.1) where we take the point with the maximum likelihood to start the chain. We draw 201000 iterations. With a burnin of 1000 and a thinning rate of 100, $K = 2000$ samples remain to approximate the posterior distribution. We get a summary for the seven data series in the boxplots in Figure 2.

We observe similar estimations for the seven data series for the parameters α and c whereas the estimations for β and a differ between the data series. This can be explained by the very different lifetimes of the experiments. The second experiment takes just over two hundred thousand load cycles, whereas the fifth and seventh take over fifteen million.

Drawing iteratively from the predictive distribution, we take the pointwise median from the samples for the counting process in (5) for a point prediction and the 0.025- and 0.975-quantile for a 95%-prediction interval, respectively. The results for the first two series are presented in Figure 3, the prediction with the exponential intensity in black lines and the corresponding result with the power law intensity in red lines. One can hardly notice any difference. The same picture for the other five data series is given in the Appendix, Section D, where also all following figures can be found for these experiments.

The next step is to estimate the parameters of the jump diffusion process, i.e., to conduct

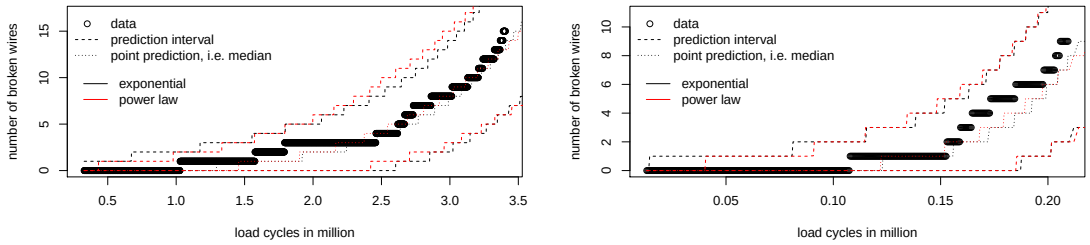

Figure 3: First (left) and second (right) data series with point and interval prediction for the counting process

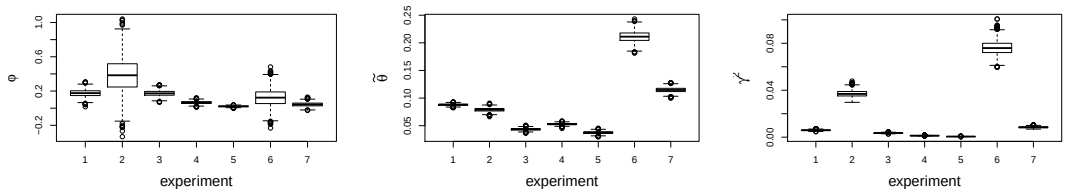

Figure 4: Boxplots for the posterior distributions of the parameters ϕ, $\widetilde{\theta}$ and γ^2 of the jump diffusion process

the Gibbs sampler. The resulting posterior distributions for ϕ, $\widetilde{\theta}$ and γ^2 are shown in Figure 4. Above all, a big difference can be seen between the second and sixth experiment and all the others. Especially the variance parameter γ^2 is estimated very high in comparison to the other series.

In Figure 5 we see the resulting predictions for the crack width process, based on the predictions for the Poisson process with the power law intensity rate (2) in red and with the exponential intensity (3) in black, again for the first two series. There were very little differences for the counting process, but there are practically no differences for the crack width process. Therefore, both intensity rates can be recommended for these data series.

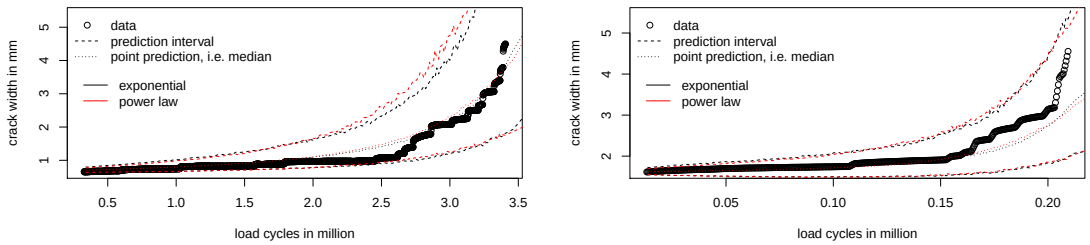

Figure 5: First (left) and second (right) data series with point and interval prediction for the crack width process

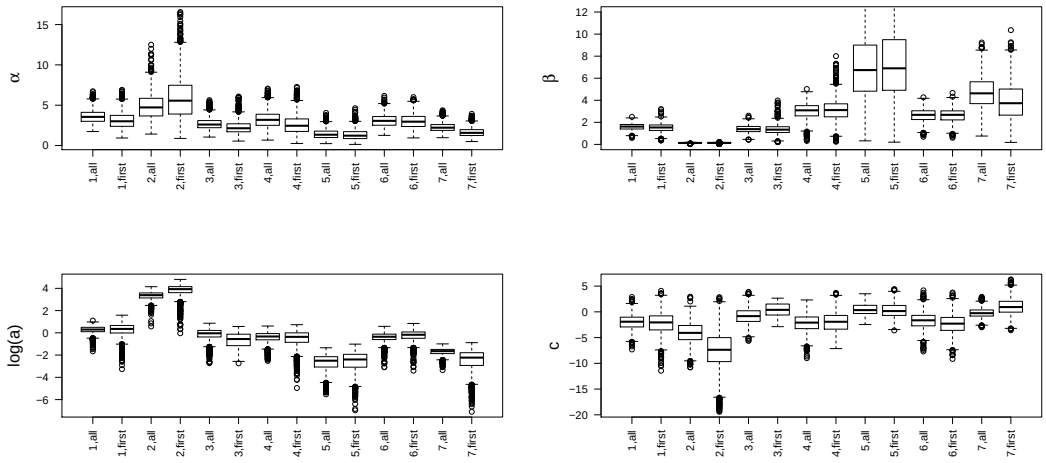

Figure 6: Boxplots for the posteriors of α and β (top) and a (in log-scale) and c (bottom) of the seven series, for the posterior conditional on the whole series on the left and for the truncated series on the right, respectively

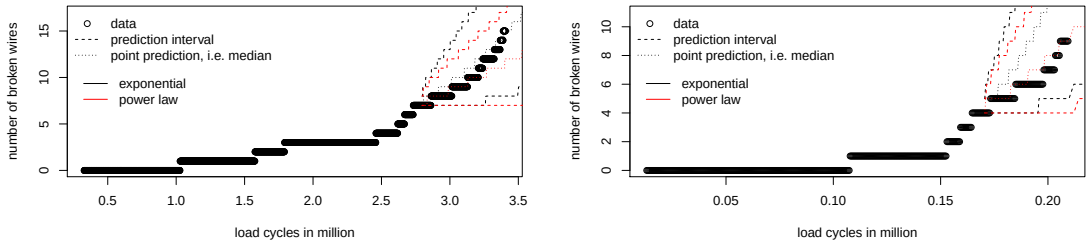

Figure 7: First (left) and second (right) data series with point and interval prediction based on a first part of the series for the counting process

As already mentioned, an important issue is the prediction of the further development at an early stage of the respective process. To investigate the model properties in this case, we use only the first part of the observed data (80% for the first five and the seventh, 90% for the sixth series) for each series. In Figure 6, we compare the posterior distributions resulting from the estimation based on the whole series ("all") and the truncated series ("first"). Except the second series, α is estimated a little smaller for the truncated series in all cases. We see the effect in the predictions given in Figure 7 for the first two experiments. In the first series, the point prediction does not follow the true curve but predicts a lower development whereas the prediction in the second series describes the true development quite well.

Figure 6 shows the comparison of the posteriors for a and c in the case of the exponential intensity (3). Except for the second experiment, the posteriors do not differ much. This is also supported by Figure 7, where the prediction with the exponential intensity for the first series follows the true curve exactly. The second curve gets overpredicted substantially because of the overestimated a.

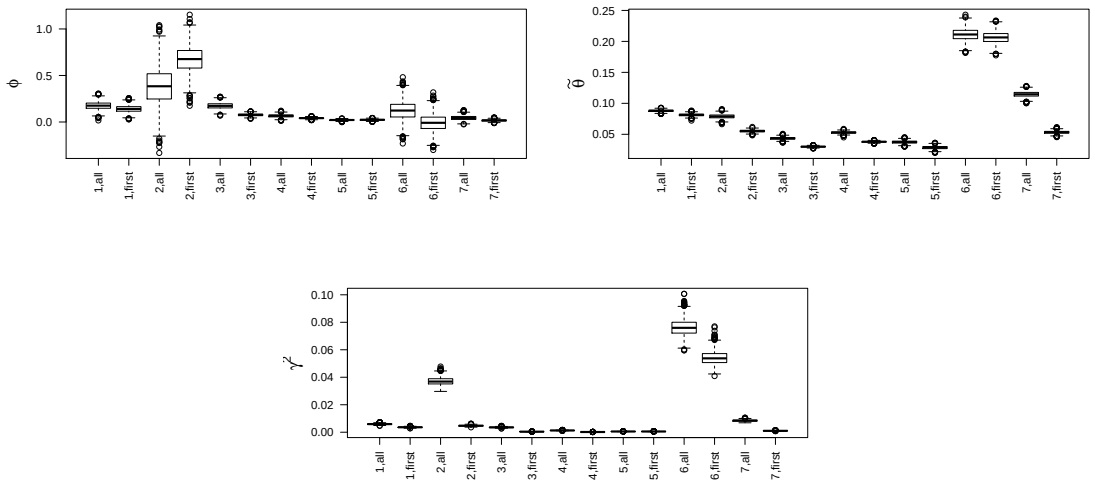

Figure 8: Boxplots for the posteriors of ϕ, $\widetilde{\theta}$ and γ^2 for the seven series, for the posterior conditional on the whole series on the left and for the truncated series on the right, respectively

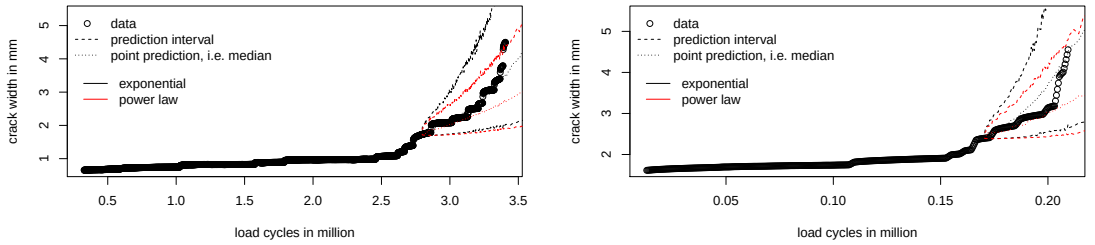

Figure 9: First (left) and second (right) data series with point and interval prediction based on the first part of the series for the crack width process

The comparison of the estimations for the parameters ϕ, $\widetilde{\theta}$ and γ^2 can be seen in Figure 8. In all cases, the estimation of the variance parameter γ^2 is a little smaller based on the truncated series. Additionally, in all cases except for the second experiment, the other parameters are estimated to lower values, as well. The result of the prediction are presented in Figure 9. In summary, we can say that the posteriors conditional on the first part of the series lead to a good prediction for the further development. While the counting process for the second experiment was overpredicted, the prediction for the crack width works well with the exponential intensity rate.

Therefore, we can say without restriction that the exponential intensity works well for the prediction of the crack width. For the prediction of the counting process, this is the case for all series except for the second. As the model will be applied to bridges and other constructions mad of prestressed concrete, it is better to predict a failure too early than too late. This leads to the recommendation to use the exponential intensity for the prediction of

the further development of the process. For a prediction of a new experiment under the same conditions, both intensity rates are equally recommendable. This result is also supported by the simulation study, which can be found in the Appendix, Section C. Beside testing the estimation and prediction scheme under known parameters, cross validation is made. It turns out that prediction based on the posterior conditional on the completely observed process works well with both intensity functions. For prediction based on the truncated series a difference is visible. The results in the case of predicting with the exponential intensity while the power law is the true underlying one are better than vise versa.

4. Conclusion

In this paper, a two-stage modeling procedure for the fatigue process in prestressed concrete is presented. Firstly, the predictive distribution for the failure process of the tension wires is calculated. For modeling this failure process, a NHPP is assumed and two intensity rates are compared, one with polynomial and one with exponential growth. It turns out that the results are comparable for both intensity functions if the aim is fitting the data or predicting a new experiment under the same experimental conditions. If the aim is predicting the further development at an early stage of the process, however, the exponential function is highly recommended. This function actually represents the Paris-Erdogan law that is well-known in the engineering literature to describe fatigue behavior.

Secondly, the predictive distribution of the NHPP, especially the uncertainty of the process, is used in the calculation of the predictive distribution of the concrete crack width process that is modeled by a jump diffusion. It turns out that for this process, the exponential intensity rate is recommendable without restrictions as well for this data set.

How to use prior knowledge of existing experiments when analyzing a new experiment under different experimental conditions will be future work. One idea is to include experimental variables like the stress range into the model. Furthermore, simultaneous prediction bands for the jump diffusion process would be preferable to pointwise intervals. The solution of this problem is not self-evident, since sampling from a multivariate distribution is needed. Moreover, from the heuristic of the counting process it would be also suitable to investigate a self-exciting process, see, for example, Ríos Insua et al. (2012) p. 125, instead of the NHPP. If a tension wire breaks, the load distributes on one wire less, which could then be included in the intensity rate that would depend on the past event times or the number of broken wires up to time t.

Acknowledgement

This work has been supported by the Collaborative Research Center "Statistical modeling of nonlinear dynamic processes" (SFB 823) of the German Research Foundation (DFG) in project B5 "Statistical methods for damage processes under cyclic load". We want to thank Professor R. Maurer and Guido Heeke for their experiments and providing us the data.

Appendix

A. Ratio for Metropolis Hastings step for γ^2

Define $k(\gamma^2) = \frac{1}{2}(\log(X)_{(n)} - \mu_n(\eta))T_n^{-1}(\log(X)_{(n)} - \mu_n(\eta))^T + b^{\text{prior}}$ with $\mu_n(\eta) = \log(x_0) \cdot 1_n + (\phi - \frac{\gamma^2}{2}) \cdot t_{(n)} + \widetilde{\theta} \cdot N_{(n)}$. The conditional posterior density of γ^2 is given by

$$
\begin{aligned}
&p(\gamma^2|\ \log(X)_{(n)}, N_{(n)}, \phi, \widetilde{\theta}) \\
\propto&(\gamma^2)^{-(\frac{n}{2}+a^{\text{prior}})-1} \cdot \exp\left(-\frac{1}{\gamma^2}\left\{\frac{1}{2}(\log(X)_{(n)} - \mu_n(\eta))T_n^{-1}(\log(X)_{(n)} - \mu_n(\eta))^T + b^{\text{prior}}\right\}\right) \\
=&(\gamma^2)^{-(\frac{n}{2}+a^{\text{prior}})-1} \cdot \exp\left(-\frac{1}{\gamma^2}k(\gamma^2)\right)
\end{aligned}
$$

and the proposal by

$$
q(\gamma^2|\widetilde{\gamma}^2, \phi, \widetilde{\theta}) = (\gamma^2)^{-(\frac{n}{2}+a^{\text{prior}})-1} \cdot \exp\left(-\frac{1}{\gamma^2}k(\widetilde{\gamma}^2)\right)
$$

This leads to the ratio

$$
\begin{aligned}
&\frac{p(\gamma^2_{\text{cand}}|\ \log(X)_{(n)}, N_{(n)}, \phi^*_{k-1}, \widetilde{\theta}^*_{k-1})q(\gamma^{2*}_{k-1}|\gamma^2_{\text{cand}}, \phi^*_{k-1}, \widetilde{\theta}^*_{k-1})}{p(\gamma^{2*}_{k-1}|\ \log(X)_{(n)}, N_{(n)}, \phi^*_{k-1}, \widetilde{\theta}^*_{k-1})q(\gamma^2_{\text{cand}}|\gamma^{2*}_{k-1}, \phi^*_{k-1}, \widetilde{\theta}^*_{k-1})} \\
=&\frac{(\gamma^2_{\text{cand}})^{-(\frac{n}{2}+a^{\text{prior}})-1} \cdot \exp\left(-\frac{1}{\gamma^2_{\text{cand}}}k(\gamma^2_{\text{cand}})\right)(\gamma^{2*}_{k-1})^{-(\frac{n}{2}+a^{\text{prior}})-1} \cdot \exp\left(-\frac{1}{\gamma^{2*}_{k-1}}k(\gamma^2_{\text{cand}})\right)}{(\gamma^{2*}_{k-1})^{-(\frac{n}{2}+a^{\text{prior}})-1} \cdot \exp\left(-\frac{1}{\gamma^{2*}_{k-1}}k(\gamma^{2*}_{k-1})\right)(\gamma^2_{\text{cand}})^{-(\frac{n}{2}+a^{\text{prior}})-1} \cdot \exp\left(-\frac{1}{\gamma^2_{\text{cand}}}k(\gamma^{2*}_{k-1})\right)} \\
=&\frac{\exp\left(-\frac{1}{\gamma^2_{\text{cand}}}k(\gamma^2_{\text{cand}})\right)\exp\left(-\frac{1}{\gamma^{2*}_{k-1}}k(\gamma^2_{\text{cand}})\right)}{\exp\left(-\frac{1}{\gamma^{2*}_{k-1}}k(\gamma^{2*}_{k-1})\right) \cdot \exp\left(-\frac{1}{\gamma^2_{\text{cand}}}k(\gamma^{2*}_{k-1})\right)} \\
=&\exp\left(-\frac{1}{\gamma^2_{\text{cand}}}k(\gamma^2_{\text{cand}}) - \frac{1}{\gamma^{2*}_{k-1}}k(\gamma^2_{\text{cand}}) + \frac{1}{\gamma^{2*}_{k-1}}k(\gamma^{2*}_{k-1}) + \frac{1}{\gamma^2_{\text{cand}}}k(\gamma^{2*}_{k-1})\right) \\
=&\exp\left(\left(\frac{1}{\gamma^{2*}_{k-1}} + \frac{1}{\gamma^2_{\text{cand}}}\right)\left(k(\gamma^{2*}_{k-1}) - k(\gamma^2_{\text{cand}})\right)\right).
\end{aligned}
$$

Because of terms in $k(\gamma^2)$ which do not depend on γ^2 we can further simplify the expression. Define $C_n := \log(X)_{(n)} - \log(x_0) \cdot 1_n - \phi t_{(n)} - \widetilde{\theta} \cdot N_{(n)}$. It holds

$$
\begin{aligned}
&2 \cdot \left(k(\gamma^{2*}_{k-1}) - k(\gamma^2_{\text{cand}})\right) \\
=&\left(C_n + \frac{\gamma^{2*}_{k-1}}{2}t_{(n)}\right)T_n^{-1}\left(C_n + \frac{\gamma^{2*}_{k-1}}{2}t_{(n)}\right)^T - \left(C_n + \frac{\gamma^2_{\text{cand}}}{2}t_{(n)}\right)T_n^{-1}\left(C_n + \frac{\gamma^2_{\text{cand}}}{2}t_{(n)}\right)^T \\
=&(\gamma^{2*}_{k-1} - \gamma^2_{\text{cand}})t_{(n)}T_n^{-1}C_n^T + \frac{1}{4}((\gamma^{2*}_{k-1})^2 - (\gamma^2_{\text{cand}})^2)t_{(n)}T_n^{-1}t_{(n)}^T.
\end{aligned}
$$

Hence the ratio is given by

$$\exp\left(\left(\frac{1}{\gamma_{k-1}^{2*}}+\frac{1}{\gamma_{\text{cand}}^2}\right)\left(k(\gamma_{k-1}^{2*})-k(\gamma_{\text{cand}}^2)\right)\right)$$
$$=\exp\left(\frac{1}{2}\left(\frac{1}{\gamma_{k-1}^{2*}}+\frac{1}{\gamma_{\text{cand}}^2}\right)\left((\gamma_{k-1}^{2*}-\gamma_{\text{cand}}^2)t_{(n)}T_n^{-1}C_n^T+\frac{1}{4}((\gamma_{k-1}^{2*})^2-(\gamma_{\text{cand}}^2)^2)t_{(n)}T_n^{-1}t_{(n)}^T\right)\right).$$

B. Algorithms

In the following we give a detailed explanation of the algorithms presented in the Sections 2.1 and 2.2.

B.1. Proposal density

The first algorithm is the Metropolis Hastings algorithm, see Robert and Casella (2004), p. 270. We use it to obtain the posterior distribution for the parameter ξ in the cumulative intensity rate of the counting process. After choosing a starting value ξ_0^*, we have to choose a proposal density. The normal distribution often is a good option and is used for c. But for a strictly positive parameter, another choice is suitable. We propose to draw a candidate $\sqrt{\xi_{cand}}$ from $\mathcal{N}(\sqrt{\xi_k^*},\sigma_p^2)$ with $\sigma_p=\frac{\sqrt{\xi_0^*}+0.1}{c}$ in the k-th step. The constant c, which determines the proposal standard deviation, is chosen with respect to the chain's autocorrelation and the acceptance rate. Then, $\xi_{cand}=\sqrt{\xi_{cand}}^2$ stems from a proposal density

$$q(\xi_{cand}|\ \xi_k^*)=\frac{1}{2\sqrt{2\pi\xi_{cand}}\sigma_p}\exp\left(-\frac{1}{2\sigma_p^2}\left(\sqrt{\xi_{cand}}-\sqrt{\xi_k^*}\right)^2\right),\ \xi_{cand}\in[0,\infty).$$

The candidate will be compared to the old value in a ratio, that means, it will be accepted, i.e. $\xi_{k+1}^*=\xi_{cand}$, if

$$u\leq\frac{p(T_1,...,T_m|\ \xi_{cand})}{p(T_1,...,T_m|\ \xi_k^*)}\cdot\frac{q(\xi_k^*|\ \xi_{cand})}{q(\xi_{cand}|\ \xi_k^*)},$$

with u drawn from a uniform density on [0,1], otherwise set $\xi_{k+1}^*=\xi_k^*$. For the chosen proposal density, the proposal ratio shrinks to

$$\frac{q(\xi_k^*|\ \xi_{cand})}{q(\xi_{cand}|\ \xi_k^*)}=\frac{\sqrt{\xi_{cand}}}{\sqrt{\xi_k^*}}.$$

B.2. Sampling NHPP

There are several procedures to simulate a NHPP proposed in the literature, see for example Lewis and Shedler (1979) or Lewis and Shedler (1976) for the specific intensity rate in (3). Here, we decided to sample the event times which uniquely determine the counting process. In the main article, we already calculated the predictive density (4). Direct sampling from this distribution can be employed by a rejection method, but for a large sample of the posteriors of ξ, this can take very long and it is difficult to find a good candidate area. Therefore, we propose the following procedure.

Firstly, assume that we want to predict a new series $T_1^*, T_2^*, ...$ dependent on the observed $T_1, ..., T_m$. We start with $T_0^* = 0$. For $i \geq 1$, the distribution function of the density

$$p(T_{i+1}^*|T_i^*, T_1, ..., T_m) \approx \frac{1}{K} \sum_{k=1}^{K} p(T_{i+1}^*|T_i^*, \xi_k^*)$$

with $\xi_1^*, ..., \xi_K^* \sim p(\xi|T_1, ..., T_m)$ is given by

$$\begin{aligned} F_{T_{i+1}^*}(t|T_i^*, T_1, ..., T_m) \approx & \frac{1}{K} \sum_{k=1}^{K} \int_0^t p(s|T_i^*, \xi_k^*)\, ds \\ = & \frac{1}{K} \sum_{k=1}^{K} F_{T_{i+1}^*}(t|\ T_i^*, \xi_k^*) =: H(t), \end{aligned}$$

where

$$F_{T_{i+1}^*}(t|\ T_i^*, \xi) = P(T_{i+1}^* \leq t|\ T_i^*, \xi) = 1 - \exp\left(-\Lambda_\xi(t) + \Lambda_\xi(T_i)\right)$$

is the cumulative distribution function of event time T_{i+1}^* and depends on T_i^*. Hence, H is explicitly given. If H^{-1} would be known, we would get samples from the distribution of H by $H^{-1}(u)$, where $u \sim \mathcal{U}(0,1)$ has the uniform distribution on [0,1]. Since H^{-1} is not calculable, we obtain $H^{-1}(u)$ by a binary search algorithm, see, for example, Gentle et al. (2012) p. 60, starting at T_i^*.

C. Simulation Study

To verify the estimation and prediction procedure we conduct a small simulation study with 1000 series. In time points $t_0 = 0, t_1 = 0.01, ..., t_{100} = 1$ we simulate one thousand Poisson processes each for the two intensity rates

$$\begin{aligned} &\Lambda_\xi(t) = \left(\frac{t}{\beta}\right)^\alpha, && \xi = (\alpha, \beta) \in [1, \infty) \times (0, \infty) \\ &\Lambda_\xi(t) = \exp(at + c) - \exp(c), && \xi = (a, c) \in (0, \infty) \times \mathbb{R}. \end{aligned}$$

Afterwards, we simulate the jump diffusion processes with the power law intensity.

C.1. Counting process

We simulate one thousand Poisson processes by drawing the event times with the distribution function

$$F_{T_{m+1}}(t|\ T_m, \xi) = P(T_{m+1} \leq t|\ T_m, \xi) = 1 - \exp\left(-\Lambda_\xi(t) + \Lambda_\xi(T_m)\right).$$

Invertation yields

$$F_{T_{m+1}}^{-1}(u|\ T_m, \xi) = \begin{cases} \beta \left(\Lambda_\xi(T_m) - \log(1-u)\right)^{\frac{1}{\alpha}} & ,\xi = (\alpha, \beta) \\ \frac{1}{a} \left(\log\left\{\exp(aT_m + c) - \log(1-u)\right\} - c\right) & ,\xi = (a, c). \end{cases}$$

Sampling the event times is employed by drawing uniform distributed u^* and take $F_{T_{m+1}}^{-1}(u^*|\ T_m, \xi)$ as a sample for $T_{m+1}, m = 0, 1, 2, ...$ until $t_{100} = 1$ is reached.

The power law intensity

For the parameters $\alpha = 5$ and $\beta = 0.5$ we see in Figure 10 the first one hundred simulated series. With the noninformative estimation approach we get through the MH-algorithm for

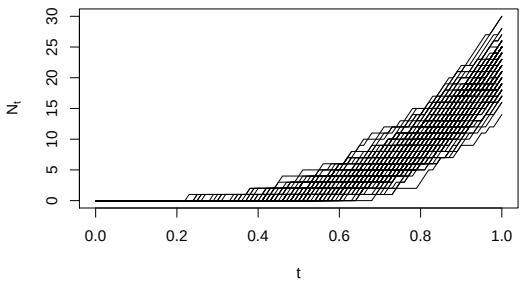

Figure 10: First one hundred simulated NHPP series with $\Lambda_\xi(t) = \left(\frac{t}{0.5}\right)^5$

each series a sample of length $K = 2000$ (201000 chain iterations, 1000 burn-in samples, thinning rate 100) where we see in Figure 11 the 95% credibility intervals exemplarily for the first one hundred series. The point inside each interval marks the point estimation, i.e. the median of the posterior distribution. 943 of all one thousand intervals for α and 945 of the intervals for β cover the true value.

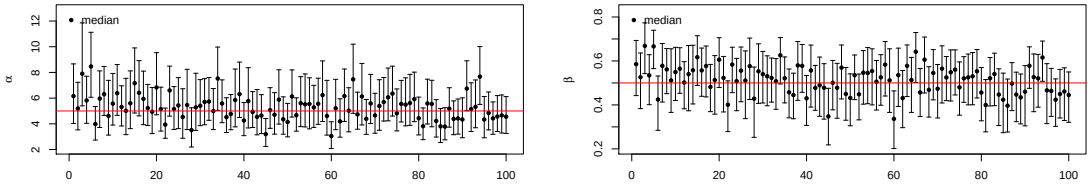

Figure 11: 95% Credibility intervals for the first 100 simulations, red: true value; coverage rate over all 1000: 0.943 for α, 0.945 for β

Based on these posterior samples as described in Section 2.1, a prediction for the NHPP series is made. The resulting samples

$$\{N_t^{*(l)} = \{j : \ T_j^{*(l)} \leq t < T_{j+1}^{*(l)}\} |\ t \in [0, \infty)\}, \ l = 1, ..., 2000,$$

are multivariate predictions for the whole series. Therefore, the pointwise 0.025- and 0.975-quantiles can be seen as simultanuous prediction bands and a coverage rate is calculated by counting how many of the simulation series are covered by their prediction bands. This is the case for 983 of the one thousand series. In addition we can investigate if an prediction interval would also cover the other simulated series what, for example, would be the case if we want to make a prediction for a new experiment under same conditions. For the one thousand intervals in average would each of them cover 69.1% of the other series.

The exponential intensity

With the same time points as before we simulate one thousand series for the NHPP with the exponential intensity rate with $a = 4$ and $c = -1$. The first hundred processes are shown in Figure 12.

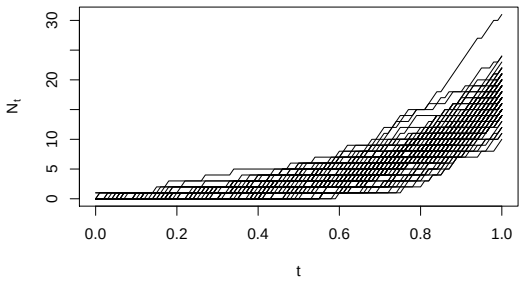

Figure 12: First one hundred simulated NHPP series with $\Lambda_\xi(t) = \exp(4t - 1) - \exp(-1)$

In Figure 13 we see similar to Figure 11 the approximated 95% credibility intervals with the corresponding point estimation for a and c for the first one hundred series. Altogether, 940 of the credibility intervals of a and 930 of the credibility intervals for c include the true value. Based on these posterior samples, 971 of the prediction bands include the true process. And each of the prediction interval bands would contain 66.2% of the other series in average.

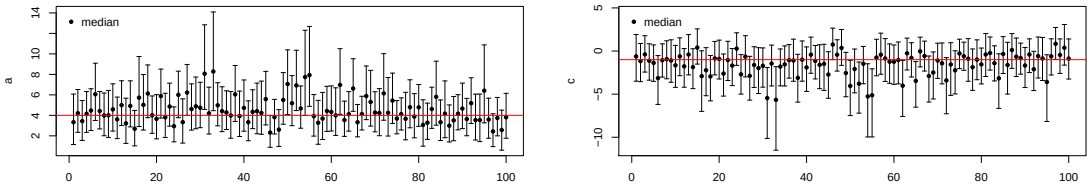

Figure 13: 95% credibility intervals for the first 100 simulation series, red: true value; coverage rate over all 1000: 0.94 for a, 0.93 for c

C.2. Jump diffusion process

The jump diffusion process presented in the main article is given by

$$X_t = x_0 \cdot \exp\left(\phi t - \frac{\gamma^2}{2}t + \gamma W_t + \log(1+\theta)N_t\right).$$

Based on this explicit solution, simulations can be derived by plugging in the series of the NHPP, samples drawn from the normal distribution for the Wiener process and the chosen

paramters $x_0 = 0.5, \phi = 0.1, \gamma^2 = 0.1^2$ and $\theta = 0.2$. In Figure 14, the first one hundred simulations based on the NHPP with the power law intensity are displayed.

Based on the Gibbs sampler, in Figure 15, the 95% credibility intervals for ϕ, $\widetilde{\theta} = \log(1+\theta)$ and γ^2 of the first one hundred series are displayed.

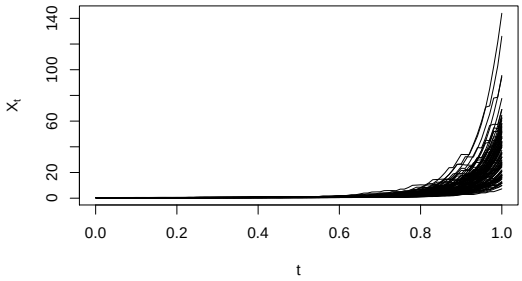

Figure 14: First one hundred simulated jump diffusion series based on the NHPP series in Figure 10

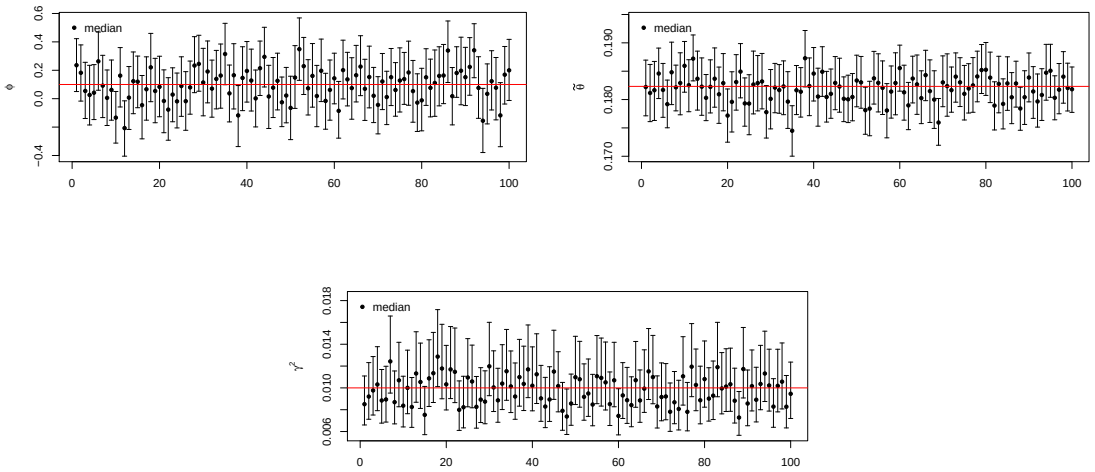

Figure 15: 95% credibility intervals for the first 100 simulations for ϕ, $\widetilde{\theta}$ and γ^2, red: true value; coverage rate over all 1000: 0.958 for ϕ, 0.959 for $\widetilde{\theta}$ and 0.941 for γ^2

Based on the posterior samples resulting from the Metropolis-within-Gibbs sampler, which is presented in the main article, and the predictive distribution samples of the NHPP, we calculate the predictions for the simulated jump diffusion series. In Figure 16 we see the pointwise coverage rates over the time. The solid line marks the amount of prediction intervals that include the simulated data point they are calculated for. In the case of prediction for a new series, it is also interesting, how many of the other simulated series are covered by a prediction interval. The dotted line in Figure 16 marks the average amount of simulated data points (999 in each time point) that are included in each prediction interval.

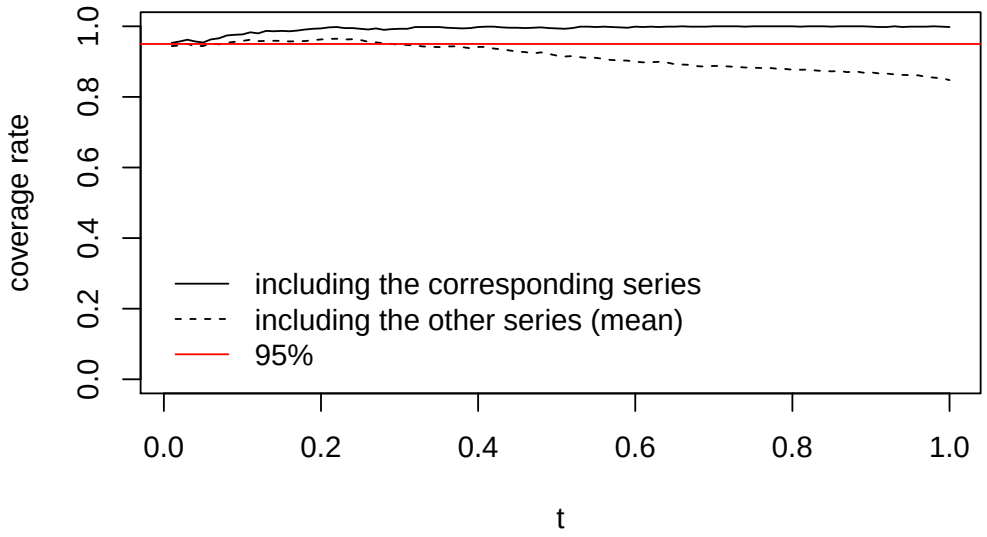

Figure 16: Pointwise coverage rate for the jump diffusion process

C.3. Cross validation

The remaining question is, how the prediction works in the case that the assumed intensity function is not the true but unknown curve underlying the data. For that investigation we take the data set simulated with the power law intensity and conduct the estimation and prediction procedure assuming the exponential one, and the other way round. Surprisingly, the effect is very small. In Figure 17 we see the coverage rates for the jump diffusion processes and they are comparable for both estimations, the true underlying and the wrongly assumed one. Therefore, if the whole series is observed, assuming a different behavior seems to be no disadvantage. The next question is, what happens in the case of predicting the further development in the case that only a first part of the series is observed. Considering that, we take only the first 81 observations of each series for the estimation and predict the last 20. The resulting coverage rates are displayed in Figure 18. The difference is very small, but the prediction with the exponential intensity in the case of the underlying power law seems to be better than vice versa.

D. Additional Figures

In Section 3, figures for the prediction results are only displayed for the first two experiments. In the following, the results for the remaining five experiments are shown. In Figure 19, we can see prediction results for the wire failure process. The difference between the two intensity rates are negligible and all interval bands include the true process. In Figure 20 we see the prediction results, which are based on the estimation with truncated series. Here, the Markov property is used and prediction is made for the further development of the series. For the

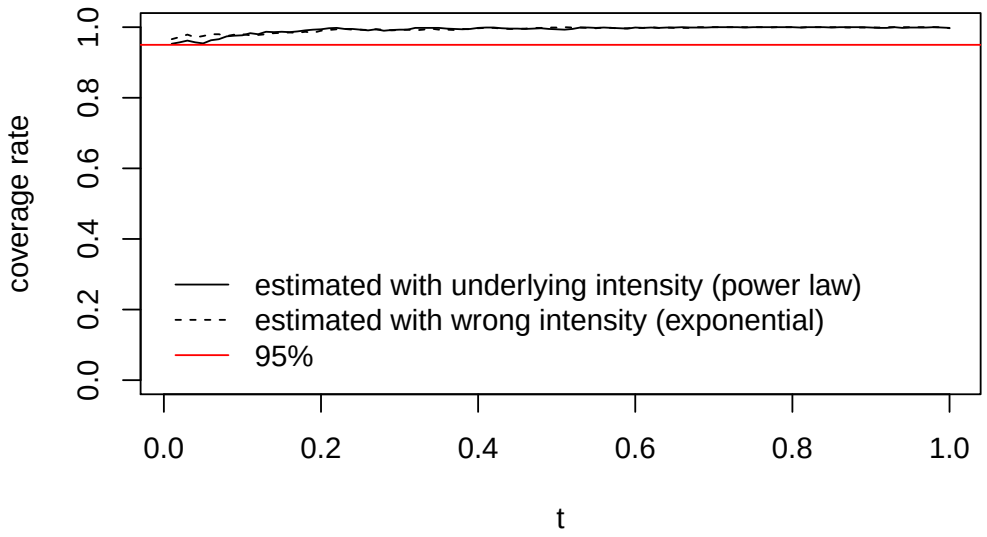

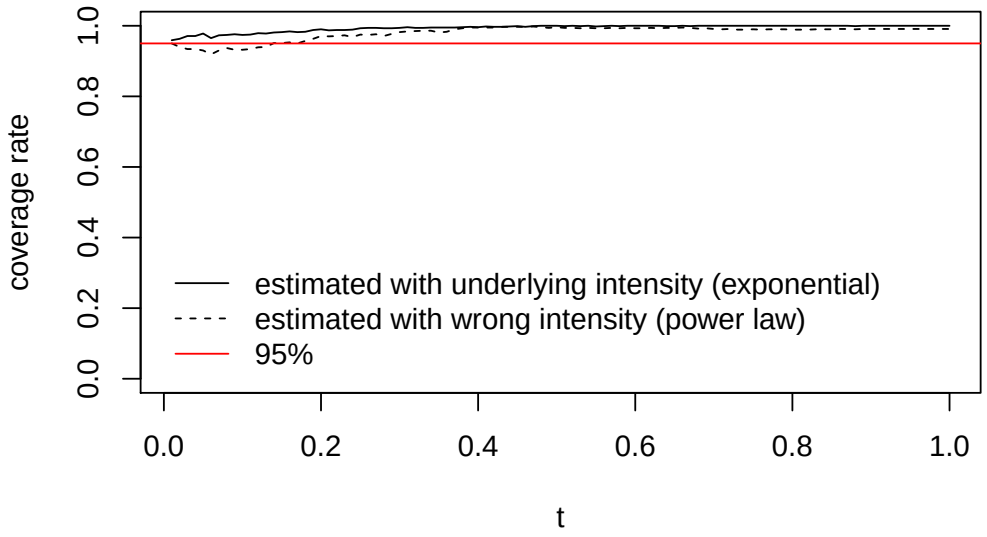

Figure 17: Coverage rates, top: for the data set simulated with the power law intensity, bottom: for the data set simulated with the exponential intensity

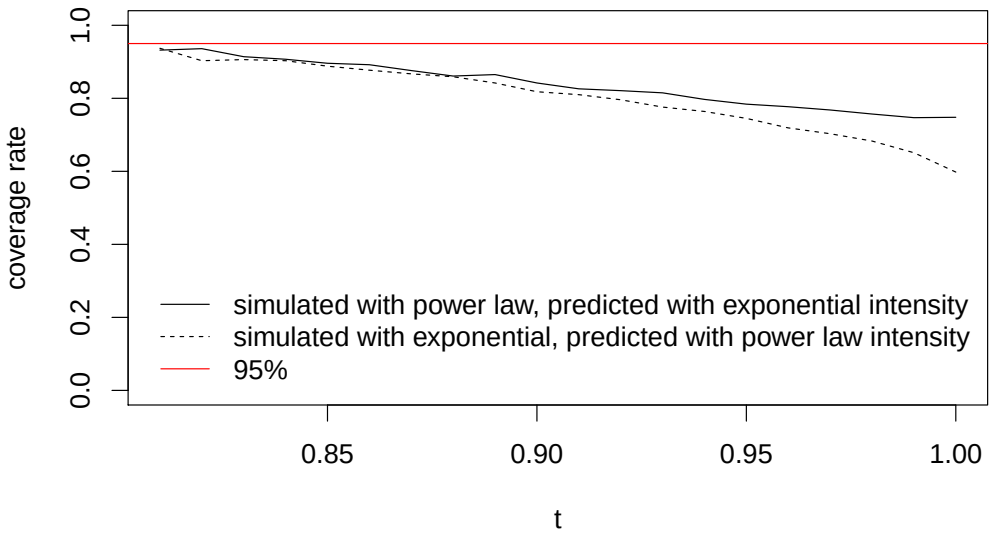

Figure 18: Coverage rates for the prediction in $t_{81} = 0.81, ..., t_{100} = 1$

third and the seventh experiment, both intensity functions lead to a prediction that is too low. But the exponential intensity yields better results than the power law function.

In Figure 21, the prediction results for the crack width process can be seen. Except some few points, the processes are well fitted. In Figure 22, we can see that for the third and the seventh experiments the prediction goes totally wrong. Reasons can firstly be found in the low prediction for the wire failure process and secondly in the very low estimation of the parameter $\widetilde{\theta}$ in comparison to the estimation with the whole series, as can be seen in Figure 8.

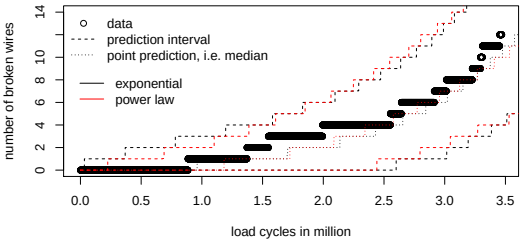

(a) Third experiment

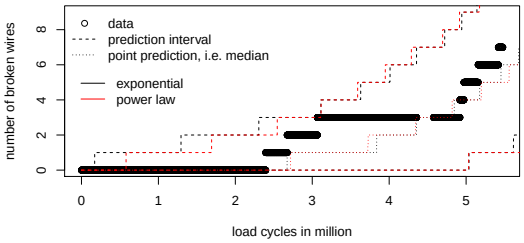

(b) Fourth experiment

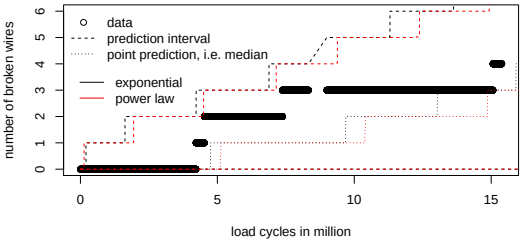

(c) Fifth experiment

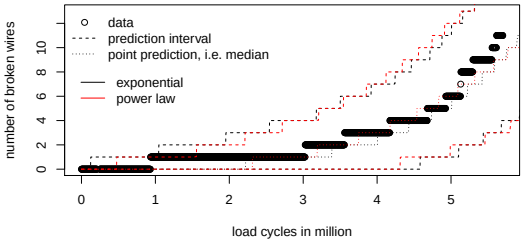

(d) Sixth experiment

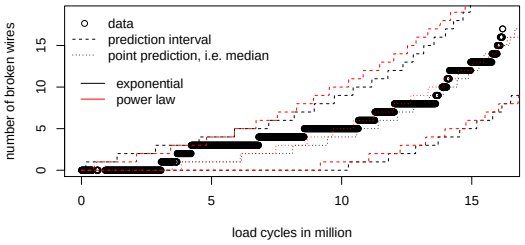

(e) Seventh experiment

Figure 19: Point and interval prediction for the counting processes

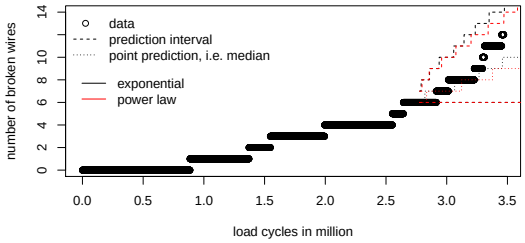

(a) Third experiment

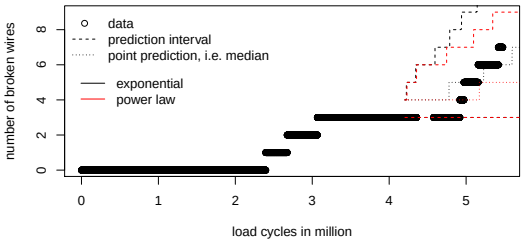

(b) Fourth experiment

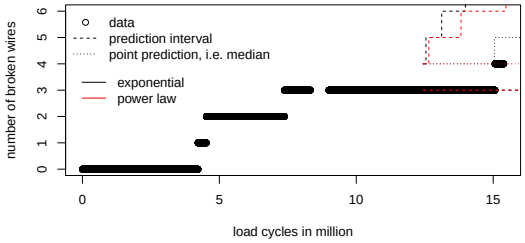

(c) Fifth experiment

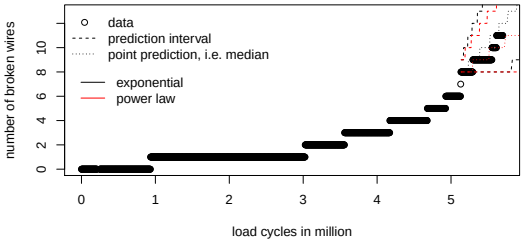

(d) Sixth experiment

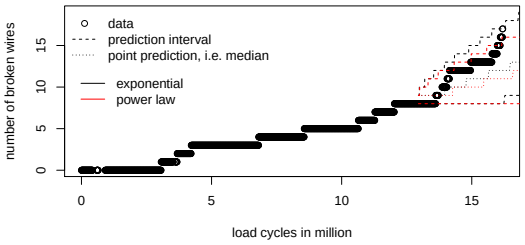

(e) Seventh experiment

Figure 20: Point and interval prediction for the counting processes

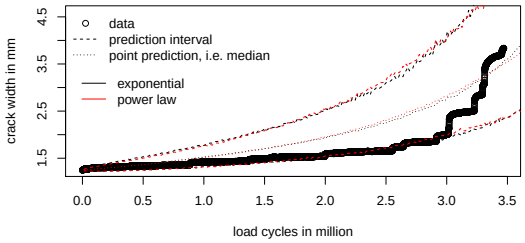

(a) Third experiment

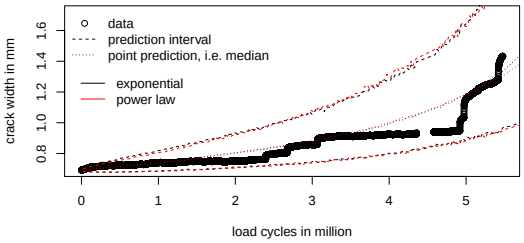

(b) Fourth experiment

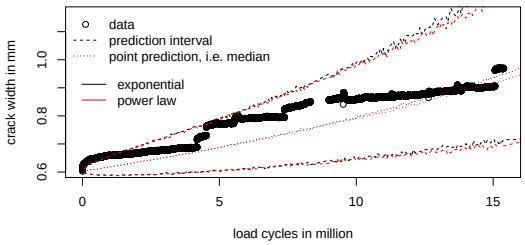

(c) Fifth experiment

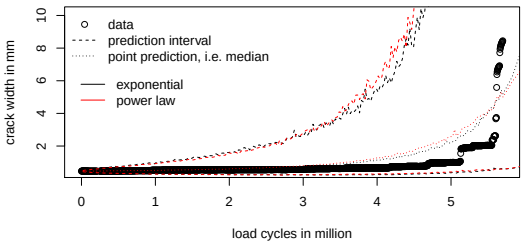

(d) Sixth experiment

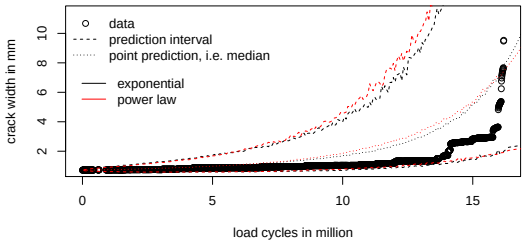

(e) Seventh experiment

Figure 21: Point and interval prediction for the crack width processes

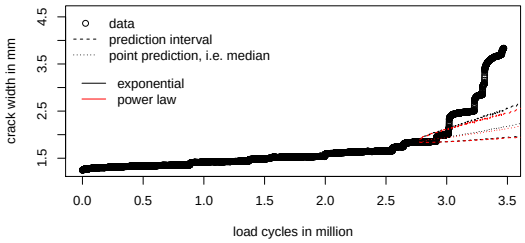

(a) Third experiment

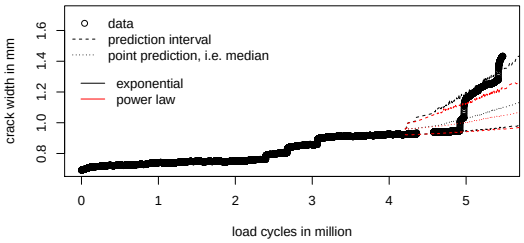

(b) Fourth experiment

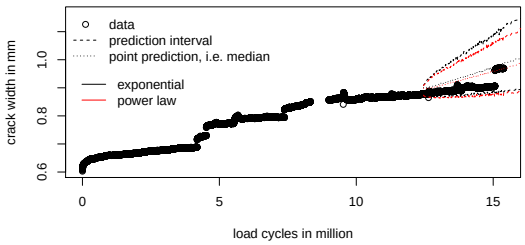

(c) Fifth experiment

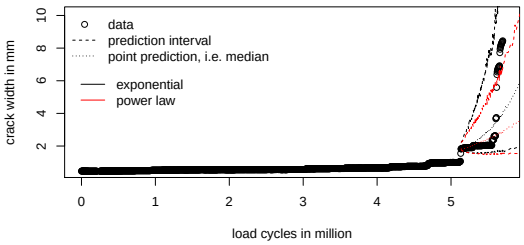

(d) Sixth experiment

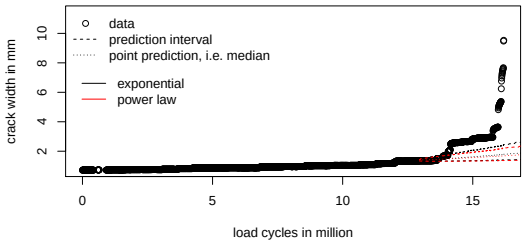

(e) Seventh experiment

Figure 22: Point and interval prediction for the crack width processes